Stability of the Mn photoluminescence in bifunctional ZnS:0.05Mn nanoparticles

Article *in* Journal of Applied Physics · August 2013

DOI: 10.1063/1.4817371

CITATIONS
35

READS
167

6 authors, including:

Juan Beltran-Huarac
East Carolina University
52 PUBLICATIONS **611** CITATIONS
SEE PROFILE

Jingzhou Wang
Intel
25 PUBLICATIONS **207** CITATIONS
SEE PROFILE

Wojciech M Jadwisienczak
Ohio University
109 PUBLICATIONS **1,943** CITATIONS
SEE PROFILE

Brad R. Weiner
University of Puerto Rico at Rio Piedras
222 PUBLICATIONS **2,925** CITATIONS
SEE PROFILE

AIP | Journal of Applied Physics

Stability of the Mn photoluminescence in bifunctional ZnS:0.05Mn nanoparticles

Juan Beltran-Huarac, Jingzhou Wang, Hiroki Tanaka, Wojciech M. Jadwisienczak, Brad R. Weiner et al.

Citation: J. Appl. Phys. **114**, 053106 (2013); doi: 10.1063/1.4817371
View online: http://dx.doi.org/10.1063/1.4817371
View Table of Contents: http://jap.aip.org/resource/1/JAPIAU/v114/i5
Published by the AIP Publishing LLC.

Stability of the Mn photoluminescence in bifunctional ZnS:0.05Mn nanoparticles

Juan Beltran-Huarac,[1,2,a)] Jingzhou Wang,[3] Hiroki Tanaka,[3] Wojciech M. Jadwisienczak,[3] Brad R. Weiner,[1,4] and Gerardo Morell[1,2]
[1]*Institute for Functional Nanomaterials, University of Puerto Rico, San Juan, Puerto Rico 00931, USA*
[2]*Department of Physics, University of Puerto Rico, San Juan, Puerto Rico 00936, USA*
[3]*School of Electrical Engineering and Computer Science, Ohio University, Athens, Ohio 45701-2979, USA*
[4]*Department of Chemistry, University of Puerto Rico, San Juan, Puerto Rico 00936, USA*

(Received 6 June 2013; accepted 17 July 2013; published online 6 August 2013)

We investigate the stability of the orange band photoluminescence (PL) of bifunctional nanoparticles of Mn^{2+}-doped ZnS at 5% (ZnS:0.05Mn). These 4-nm nanoparticles are synthesized via a one-step inorganic chemical route under ambient conditions. The phase, crystallinity, and morphology are analyzed via X-ray and electron diffractions and high-resolution electron microscopy. Based on the thermally activated carrier-transfer model, it is found that orange emission is rather stable at low temperatures and possesses thermal activation energy of ~18 meV. The analysis of the PL decay curves suggests the coexistence of multiple lifetimes, that the shortening observed in PL lifetime is not due to the Mn^{2+} ions, and that the orange band decay is stable in temperature range from 10 K to 300 K. The measured *M-H* hysteresis loops demonstrate that ZnS:0.05Mn nanoparticles exhibit ferromagnetic ordering below 30 K, unlike its bulk counterpart. No magnetic field dependence of the Mn^{2+} PL intensity is observed up to 1 T. The stability of the PL signal when subject to an applied magnetic field is discussed. This study offers experimental evidence to test low-dimensional dilute magnetic semiconductor models and widens the range of applications of ZnS:Mn nanostructures beyond optoelectronics. [http://dx.doi.org/10.1063/1.4817371]

I. INTRODUCTION

Transition-metal doped semiconductor nanocrystals have been the focus of intensive investigation during the past few decades owing principally to the synergistic advantage offered by the incorporation of these types of impurities into host semiconductors. It has been widely established that in dilute magnetic semiconductors (DMSs) of groups II–VI no extra charge carriers are introduced in the host semiconductor by magnetic transition-metal impurities, which allow us a better understanding of many processes such as carrier relaxation, energy and spin transfer, and multiplicity of decay times.[1] The controlled incorporation and homogeneously dispersed distribution of these impurities have led to unusual phenomena being directly observed, such as large Faraday rotation, zero-field magnetization, magnetic-field induced metal-insulator transition, exciton-Mn^{2+} complexes, and giant Zeeman splitting.[2] Additionally, DMS nanoparticles undergoing quantum confinement have been shown to induce not only amenable size-dependent optical and electronic properties but also magnetic ordering below the Curie temperature, T_C.[3] The type of interaction between magnetic ions and quantum confined carriers is likely mediated by the hybridization of the impurity *d* level with the valence and conduction bands of the host lattice.[4] Various accounts to elucidate the hybridization mechanism have been up to now reported, but they lack substantial experimental support.[5] Even though nanocrystals of DMSs may exhibit better bifunctional performance than their bulk counterparts, only a few known systems have been thoroughly studied to date.[6,7]

Mn^{2+} doped ZnS (ZnS:Mn) nanoparticles have been studied by many research groups due to their prominent properties, such as high photoluminescence (PL) efficiency and lifetime shortening[8–10] attributed to the prominent exchange interaction between the *sp* band electrons of the nanocrystal and the *d* electrons of the Mn^{2+}ions. In addition, a confinement-induced ferromagnetic ordering has been predicted in ZnS:Mn nanocrystals through first-principles calculations.[3] Recently, ferromagnetism in ZnS:Mn below 30 K has been experimentally observed.[11,12] However, there are no additional reports confirming such ferromagnetic ordering. More emphasis has been devoted to investigating the mechanism whereby the spin-forbidden $^4T_1$-$^6A_1$ transition of the Mn^{2+} becomes less spin forbidden, which would result in a shorter decay time and a faster energy transfer through a plausible hybridization process.[8] However, the origin of the improved PL efficiency due to a shorter lifetime in ZnS:Mn nanoparticles is still debated and controversial. Although PL data of ZnS:Mn have been extensively studied, its corresponding magnetic ordering remains uncorrelated giving rise to conflicting and confusing interpretations.[8–10]

Recently, a suppression of the orange band PL intensity has been reported for ZnS:Mn nanoparticles in their ferromagnetic state by applying a magnetic field up to 50 T.[11] In the same study, a significant temperature-dependent variation of

a)Author to whom correspondence should be addressed. Electronic mail: baristary26@gmail.com

the Mn PL intensity of ZnS:Mn was also observed in both the ferromagnetic and paramagnetic phases in the absence of an applied magnetic field. Further investigation is, however, required to understand the magneto-luminescent (ML) coupling, which requires huge magnetic fields. Moreover, additional experimental evidence is needed to properly correlate the relaxation processes and carrier-transfer mechanisms in ZnS:Mn nanoparticles with their intriguing ferromagnetic ordering. Such correlations would bring forth new vistas to extend the scope of applications of ZnS:Mn in optoelectronics and spintronics.

We report here a systematic study on the low-temperature bifunctional properties of ZnS:0.05Mn nanoparticles with average 4-nm diameter. Based on the experimental findings of the observed bifunctional behavior, we show that the manganese PL of ZnS:0.05Mn in its ferromagnetic state under the influence of a moderated magnetic field is stable. A plausible explanation for this stability is also presented.

II. EXPERIMENTAL SECTION

A. Synthesis of ZnS:0.05Mn nanoparticles

Mn^{2+}-doped ZnS nanoparticles were synthesized via a one-step inorganic chemical route reported elsewhere.[13] Briefly, 3.227 g of $ZnSO_4{\cdot}H_2O$ and 0.162 g of $MnSO_4{\cdot}H_2O$ were dissolved into 90 ml of high-purity deionized water (HPD), resulting in a 5 wt. % Mn doping. An aqueous solution of Na_2S (1.404 g, 90 ml) was separately prepared and gradually dripped into the first aqueous solution *in vacuo* with a pH adequately adjusted, and then vigorous magnetic stirring was maintained at room temperature (RT) with a controlled reflux system. The reagent mixture rapidly produced a deep orange solution when exposed to UV light indicative of the compound formation. The flocculate was then removed from the supernatant by ultracentrifugation. The resulting solution was further ultracentrifuged and copiously rinsed with HPD, and dried at 330 K for 24 h in order to eliminate any remaining by-product. The doping level used for this inorganic synthesis route provides a broad defect-related ZnS band similar in intensity to that obtained by standard procedures (solvothermal route at Mn^{2+} at. 2%) at RT. Further, cylindrical pellets of ZnS:0.05Mn powder were prepared (reported elsewhere[14]) to conduct PL and SQUID measurements at low temperatures. Such pellets were fabricated using a hydraulic press under an isostatic uniaxial pressure of 3.7×10^9 N/m^2. No binder was employed. The 25 mm-diameter pellets were then heated up at 370 K to remove any surface contamination.

B. Characterization

The phase of ZnS:0.05Mn was analyzed using an X-Ray Diffractometer (XRD), Model Siemens D5000, using *Cu-Kα* radiation with $\lambda = 0.154315$ nm. A JEOL JEM-2200FS high-Cs probe-corrected high-resolution transmission electron microscope (HR-TEM) operated at 200 kV was used for imaging. Optical absorption spectra were recorded using a UV-Vis spectrophotometer (DU 800, Beckman Coulter). To collect temperature-dependent PL spectra, the samples were first mounted on the cold-finger of a closed-cycle helium-cryostat operating from 10 K to 300 K in high vacuum condition (<0.1 mPa). The samples were then excited with a 325-nm He-Cd laser (Model IK 3202 R-D) with a maximum power of 16 mW. The PL signal of the samples was dispersed by a 0.3 m Acton spectrometer with changeable holographic gratings and analyzed by a Princeton Instrument PI-MAX CCD camera equipped with UV intensifier, operating in the spectral region 200–950 nm. The decay curves were obtained by exciting the samples with an intensity-modulated He-Cd laser beam using an acousto-optic light modulator (Model AOM-125U) with a maximum modulation frequency of 125 MHz. A pulsed N_2 laser (Model UV22) operating at 337 nm with full width at half maximum of ~20 ns was used for the fast PL kinetics measurements. The time-dependent PL signals were collected by an HR320 spectrograph (0.32 m) with a *Czerny-Turner* configuration, detected by a photomultiplier (Hamamatsu R316-02) and a photon counting system with a turbo-multichannel scaler (Turbo-MCS, EG&G, Ortec), which offers a wide range of channel dwell time (minimum 5 ns) with no dead time between channels. Magnetic properties were collected using a SQUID magnetometer (Quantum Design, San Diego, CA, USA) operating in a field range from ±70 kOe and a temperature range from 10 K to 300 K. To record the ML spectra, the samples were placed on a cold stage of closed cycled cryostat (Model 202-E) coupled to an electromagnet (Lake Shore, Model EM4-HVA). The magnetic field strength was monitored with a Gaussmeter (Lake Shore, Model 475-DSP). The long-term magnetic field stability was 0.001 T and no magnetic field strength drift was observed during data collection. The temperature in ML measurements was monitored using a Lake Shore 340 temperature controller with a stability of 1 K. The ML signal was detected by using a fiber optic spectrometer (Ocean Optics, Model USB2000). The ML spectra were collected in longitudinal magnetic field geometry.

III. RESULTS AND DISCUSSION

Figure 1 shows the formation and morphology of ZnS:0.05Mn. Both XRD patterns and selected area electron diffraction (SAED) rings show three major diffraction planes (111), (220), and (311), which are indexed to ZnS spharelite according to the standard cards (JCPDS No. 77-2100) as shown in Figure 1(a). Both techniques confirmed that ZnS:0.05Mn crystallized preferentially in the cubic ZnS phase. No lattice distortion (shift) was observed in the host ZnS indicative of the successful random substitution of Mn^{2+} into Zn^{2+} sites at this doping level (Mn at. 5%). Neither parasitic phases nor signal of ZnS wurtzite was observed suggesting that the ZnS:0.05Mn sample grown by this method possesses a high degree of purity. The calculated lattice constant of ZnS:0.05Mn was $a = 0.5384 \pm 0.0007$ nm consistent with the standard value.[15] The prominent broadening of the diffraction peaks is attributed to the nanocrystalline nature of the sample. The calculated average crystallite size was determined by means of Scherrer's formula, yielding a value of 4 nm. The UV-vis absorption and PL spectra of ZnS:0.05Mn at RT are depicted in Figure 1(b). It was found that the absorption band edge position (~315 nm)

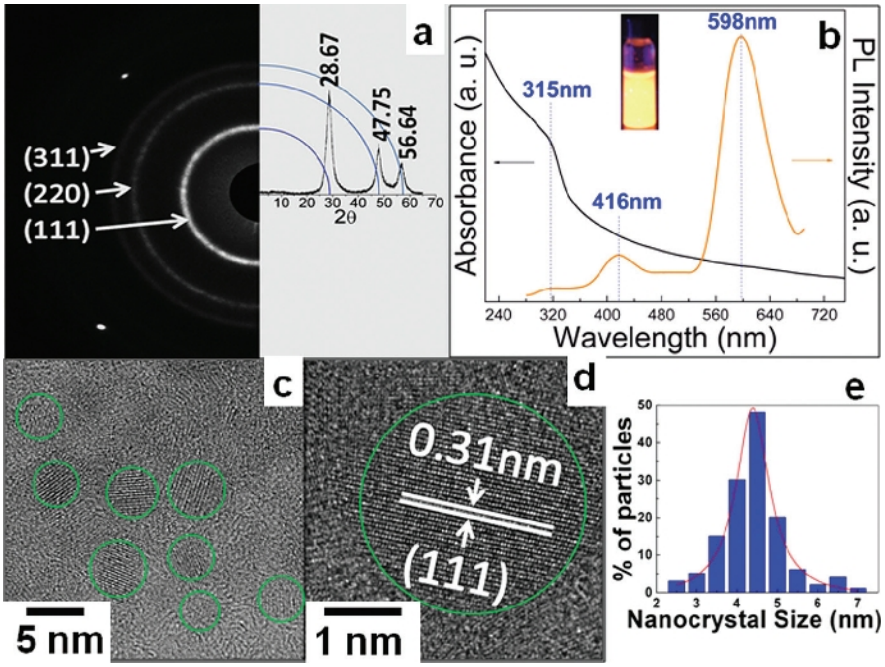

FIG. 1. (a) XRD patterns and SAED rings, (b) PL and UV-Vis absorption spectra at room temperature (inset: optical image exposed to 325 nm UV light), (c) HRTEM images of well-dispersed nanoparticles and (d) its corresponding close-up, and (e) the particle size distribution of 4-nm ZnS:0.05Mn.

does not change owing to the doping process. The blue band at ~416 nm is ascribed to the donor-acceptor pair transitions in ZnS host. The orange emission band (see the inset of Figure 1(b)) at around 598 nm is due to the internal Mn^{2+} ion transition between the $^4T_1$ first excited state with spin 3/2 and the $^6A_1$ ground state with spin 5/2, which causes energy transfer from *s-p* electron-hole pair band states (host ZnS nanocrystal) to the Mn^{2+} ion *d*-electron states.[16] Both UV-vis absorption and PL spectra confirmed the homogeneous incorporation of Mn^{2+} ions into the ZnS host. Figures 1(c) and 1(d) depict the HRTEM images of as-synthesized ZnS:0.05Mn. These images show well-dispersed spherical nanoparticles with a high degree of crystallinity whose sizes range from 2 to 7 nm. The lattice fringes were easily observed thereof. Figure 1(d) shows a closer look of a ZnS:0.05Mn nanoparticle of around 4 nm with *d*-spacing of 0.31 nm corresponding to the major plane (111) of ZnS as shown in the XRD patterns and SAED rings. The particle size distribution (see Figure 1(e)) obtained by image analysis further confirmed that the average size of these particles was around 4 nm, which is consistent with the XRD analyses.

Further studies have been conducted to analyze the temperature-dependent behavior of both emission bands in ZnS:Mn. Figure 2(a) shows the PL spectra of ZnS:0.05Mn recorded between $T = 10$ K and 300 K. The blue emission band from 4-nm ZnS:Mn nanoparticles suspended in solution

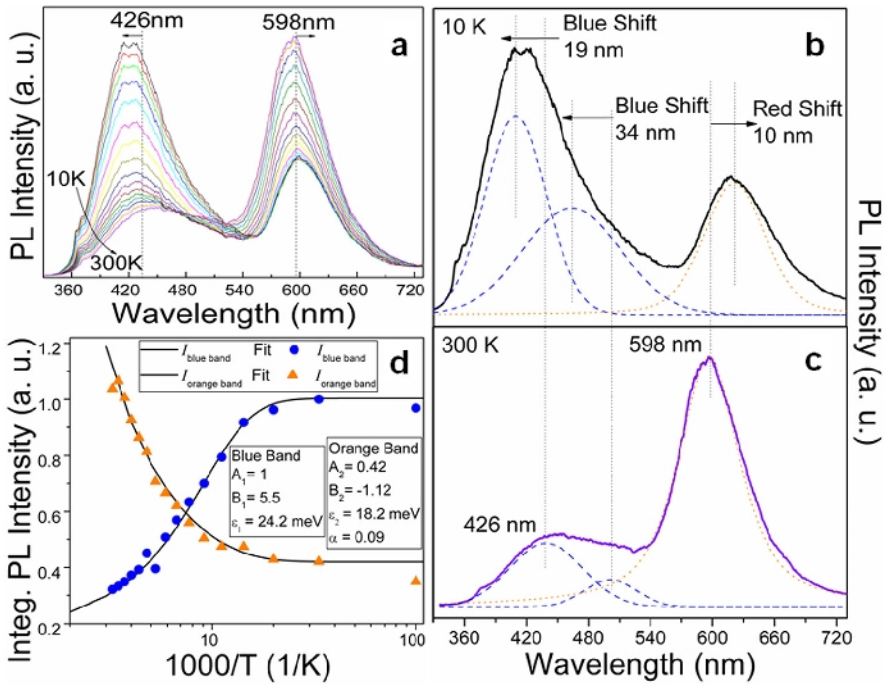

FIG. 2. (a) Temperature-dependent PL spectra of 4-nm ZnS:0.05Mn excited at 325 nm, (b) blue PL band components at 10 K (dashed lines) and (c) orange PL band components at 300 K (dotted lines) obtained from deconvolution of their respective PL spectra, (d) blue (●) and orange (▲) PL emission band intensity evolution as a function of temperature fitted to Eqs. (1) and (2) (solid lines) of 4-nm ZnS:0.05Mn.

centered at ~416 nm redshifts to ~426 nm. This upshift is presumably ascribed to the cluster-induced effect arising from the conversion of ZnS:0.05Mn powder into pellet.[17] Thus, it is believed that the donor states implicated in the blue emission are mainly linked to the nanoparticle surface states. In addition, it was found that both emission bands undergo a different evolution as the temperature is varied from 10 K to 300 K. The blue emission band undergoes a prominent rise in PL intensity and is blue-shifted as the temperature decreases.

However, the orange emission band experiences a significant drop in PL intensity and is weakly red-shifted as the temperature decreases. Similar findings were previously reported for ZnS:Mn nanoparticles smaller than 5 nm.[18,19] To gain more insight about the evolution of the emission bands with the temperature, the deconvolution of both bands at 10 K and 300 K was carried out (see Figures 2(b) and 2(c)). Two components were identified, one sub-band (major band) at ~426 nm and the other (minor band) at ~500 nm, associated to the blue band at 300 K. It was found that the temperature-dependent behavior of both the blue band and their components is similar, i.e., the major and minor blue bands are blue-shifted 19 nm and 34 nm, respectively, as the temperature decreases. The integrated blue band PL intensity was found to be 3 times larger at 10 K than at 300 K. In comparison, a redshift of 10 nm was observed in the orange band peak position when temperature changed from 300 K to 10 K. The integrated orange band PL intensity was halved from 300 K to 10 K. Figure 2(d) shows the temperature-dependent behavior of the integrated PL intensities of both major bands (normalized to the strongest PL signal of the dominant blue band). A negligible decrease in intensity of the blue band was observed over the temperature range from 10 K to 50 K. This is probably associated to non-radiative recombination processes, which are weakly temperature-dependent and is not related to the carrier transfer from donor states to Mn^{2+} ions.[18] A prominent drop in intensity was observed at higher temperatures which may result from the electrons trapped in the donor states that are thermally activated towards the conduction band.[19] Unlike the temperature quenching of the blue band at 426 nm, the orange band at 598 nm showed a continuous increase in PL intensity when temperature increased from 10 K to 300 K. This can be described by means of the carrier transfer from donor states to Mn^{2+} ions. Since the conduction electrons can move freely in the particles, some of them may be captured by the Mn^{2+} ions and then increase the $^4T_1$-$^6A_1$ transition probability as the temperature increases.[18,19] To corroborate such an energy-transfer mechanism and determine the thermal activation energy, the experimental data were simulated through a thermally activated carrier-transfer model[20] via

$$I_{blue} = \frac{A_1}{1 + B_1 \exp\left(-\frac{\varepsilon_1}{k_B T}\right)}, \quad (1)$$

$$I_{orange} = \frac{A_2 + \alpha I_{blue} B_1 \exp\left(-\frac{\varepsilon_1}{k_B T}\right)}{1 + B_2 \exp\left(-\frac{\varepsilon_2}{k_B T}\right)}, \quad (2)$$

where A_n, B_n, ε_n, α, and k_B are parameters related to the generation rates, the ratios of the nonradiative rate to the radiative rate, the activation energies for the thermal quenching, the capture factor, and the Boltzmann constant, respectively. The subscript ($n = 1,2$) stands for the blue and orange bands, respectively. The obtained fitting values by this procedure are shown in the inset of Figure 2(d). The thermal activation energies of 24 meV for the blue band and 18 meV for the orange band are comparable to those previously reported.[18] According to these values, the donor level involved in the blue emission is located around 24 meV under the conduction band edge. Nevertheless, these values are smaller than those reported for 10 nm-sized ZnS:Mn particles, which contradicts the assumption that the thermal quenching energy in Mn^{2+} is independent of the particle diameter. This variation may be ascribed to the weaker binding of excitons to the Mn^{2+} ions in smaller nanoparticles.[18] This fact was further confirmed by the value obtained for the capture factor, $\alpha = 0.09$. Given that the parameter α describes the process whereby the Mn^{2+} ions capture the thermally activated electrons from the donor state, it seems reasonable to assume that such electrons are more easily captured by Mn^{2+} ions in 4-nm ZnS:Mn particles than in larger ZnS:Mn particles. Thus, it is believed that Mn^{2+} ions are closer to the particle's surface by increasing the surface-to-volume ratio of a nanoparticle. Similar findings were reported and attributed to the carrier-transfer mechanism, which likely dominates the temperature-dependent behaviors of both emission bands.[18,19] Hence, our experimental observations suggest that the suppression of the PL orange band intensity is due to a purely thermal effect.

The PL decay curves for blue and orange emission bands were analyzed using two modulated semi-square He-Cd and N_2 laser pulses having significantly different excitation pulse rise and decay dynamics. The PL kinetics of the orange emission band was studied by exciting the 4-nm ZnS:0.05Mn with semi-square excitation pulses having 90 ns rise and 100 ns fall times, and a pulse duration of 600 μs necessary to excite the majority of Mn^{2+} ion emitting centers and to achieve steady-state excitation conditions. Figure 3

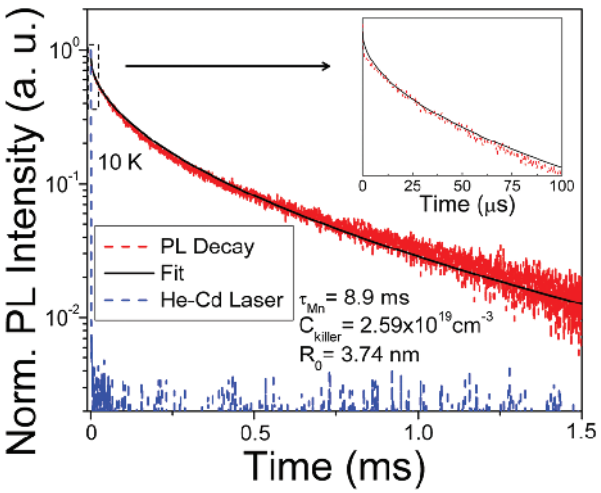

FIG. 3. PL decay curve of orange emission band of 4-nm ZnS:0.05Mn (red curve) and He-Cd laser excitation pulse decay (blue dashed curve) fitted with Eq. (3) (black solid line). Inset shows the PL decay curve between 0 and 100 μs.

depicts the PL decay curve measured for the orange band at 10 K; the laser pulse decay is shown for comparison. No difference was observed in the PL decay curve upon increasing the temperature up to 300 K (not shown here).

This PL decay curve shows a marked non-single exponential behavior, initially with a very fast PL decay (see inset of Figure 3) and followed by a slower decay at later times. This tendency typical for ZnS:Mn nanostructures is comparable to those reported by other research groups.[1,21,22] In order to gain more insight into the PL kinetics of ZnS:0.05Mn and determine the intrinsic Mn^{2+} ion decay times, the experimental data were fitted[21] following the Förster's modified model[1,23] (see fitting curve in solid line of Figure 3) via

$$\left\langle \frac{I(t)}{I_0} \right\rangle = \exp\left(-\frac{t}{\tau_{Mn}}\right) \sum_{N=0}^{\infty} p(N,\tilde{N}) \times \exp\left(-\sqrt{\pi}\frac{NV_0}{V_{sphere}}\sqrt{\frac{t}{\tau_{Mn}}}\right), \quad (3)$$

where τ_{Mn} is the intrinsic lifetime of an excited Mn^{2+} ion. The parameter N represents the number of killer centers (defects) in the material and is given by $C_{killer} = N/V_{sphere}$, where C_{killer} is the average killer center density and V_{sphere} is the volume of the spherical particle with diameter d_{sphere}. The parameter V_o is related to R_o, which is defined as a volume representing the distance from the Mn^{2+} ion to the killer center, in the form of $V_o = (4\pi/3)R_o^3$. The term $p(N,\tilde{N})$ stands for the Poisson's distribution ($N = 0,\ldots\infty$) valid when $\tilde{N}$ is much smaller than the number of atoms per dot. The fitting of the PL decay curve to Eq. (3) produced values of $\tau_{Mn} = 8.9$ ms, $R_o = 3.74$ nm, and $C_{killer} = 2.59 \times 10^{19}$ cm^{-3}. This fit reveals initially a fast multi-exponential intrinsic Mn^{2+} ion lifetime (see inset of Figure 3) as previously reported.[8] For the spectral region where the band tail predominates, a longer lifetime of 8.9 ms is observed, which is principally due to electron scattering processes. This value is longer than that reported for 9-nm ZnS:Mn nanoparticles,[1] which may be due to the size dependence of the decay lifetime. The obtained value of the average killer density, $C_{killer} = 2.59 \times 10^{19}$ cm^{-3}, is also greater than the reported value in Ref. 1, and is probably associated to a larger concentration of intrinsic defects and/or surface states existing in synthesized semiconducting 4-nm ZnS:Mn particles. Although the energy transfer from an excited Mn^{2+} ion to a killer center is mediated by a dipole-dipole interaction, the inter-sphere coupling among nearby spheres likely happens in samples with small nanoparticle size since the value of R_o is larger or comparable with the sphere diameter.[1] Furthermore, it was found that the orange band PL decay is stable over the range of temperatures studied here.

We have attempted to study the PL kinetics of the blue emission band at 426 nm observed in 4-nm ZnS:0.05Mn^{2+} using the same excitation conditions as for the orange band PL decay; however, the semi-square excitation pulses kinetics were too slow for studying the blue band PL decay. Thus, a pulsed nitrogen laser operating at 20 Hz and generating pulses with 50 ns at full width at half maximum was employed to excite the 4-nm ZnS:0.05Mn particles. No lifetime in the order of ms was observed. In addition, a lifetime much faster than that of the orange band and comparable to the N_2 laser excitation pulse decay was found (not shown here). This suggests that the shortening in PL decay time from ms in bulk to ns in nano-sized ZnS:Mn is not due to the Mn^{2+} but rather to the overlapping of the tail of broad defect-related ZnS band and the Mn^{2+} ion band as proposed in Bhargava and Gallaguer's pioneering work.[8] Similar controversial findings were found by Bol *et al.* and Godlewski *et al.*;[21,24] the controversy is not yet settled.

The magnetic hysteresis loops of ZnS:0.05Mn nanoparticles at 30 K, 40 K, and 300 K are displayed in Figure 4(a). A diamagnetic behavior was observed in the range from 100 K to 300 K, whereas a paramagnetic behavior within 40 K-90 K, as reported earlier for ZnS:Mn.[25,26] A prominent magnetic ordering was observed in the range from 10 K to 30 K.[11,12] A closer look of the *M-H* hysteresis curve at 30 K is shown in the inset of Figure 4(a) from which a coercive field of 0.2 kOe was estimated. It is known that the transition from a paramagnetic state to an ordered magnetic state is a characteristic feature of nanoparticle ensembles[12] and entails a blocking temperature, T_B. The T_B estimated from 10 K to 90 K was approximately 35 K. The existence of hysteresis with finite coercivity below that temperature implies that 4-nm ZnS:0.05Mn nanoparticles present ferromagnetic ordering. It is worth mentioning that bulk ZnS:0.05Mn does not show any evidence of ferromagnetism.[27] The origin of such ferromagnetism in highly confined systems is attributed to the formation of non-interacting magnetic polarons.[28,29] This finding is consistent with the picture of non-interacting

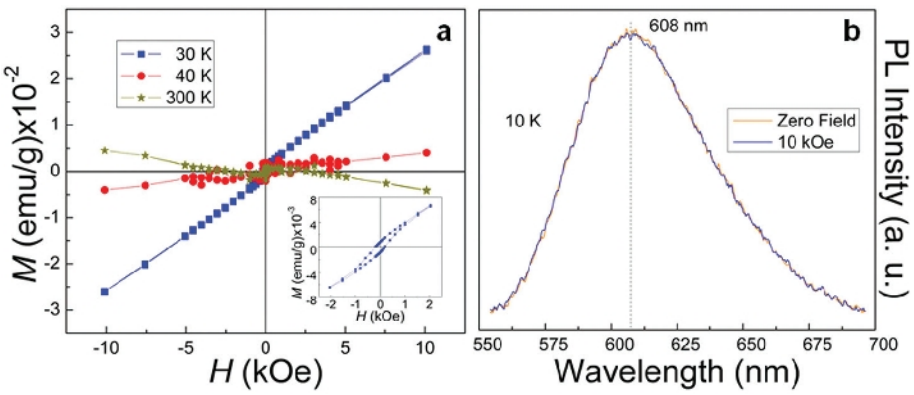

FIG. 4. (a) *M-H* hysteresis curves of 4-nm ZnS:0.05Mn at 30 K, 40 K, and 300 K. Inset shows the *M-H* loop with ±2 kOe magnetic field at 30 K. (b) PL spectra of 4-nm ZnS:0.05Mn collected at 10 K in absence (red curve) and under the influence of a magnetic field of 10 kOe (blue curve).

highly confined polarons and dipole-dipole interaction in nanoparticles.

The PL spectra of 4-nm ZnS:0.05Mn nanoparticles at 10 K in absence and under the influence of an applied magnetic field are depicted in Figure 4(b). The reference PL spectra were measured before (0 kOe) and immediately after applying a magnetic field of 10 kOe (1 T). Special precautions were taken to eliminate ambient temperature fluctuation (±1 K), laser beam intensity drift (±0.001 mW), and magnetic field instability (±10 Oe) over an extended period of time (>60 min) during the measurement of the magneto-optic PL spectra. As can be seen from Figure 4(b), the PL spectra measured prior to magnetization and after magnetization of the ZnS:0.05Mn nano-particles with 10 kOe magnetic field are identical. It should be mentioned that misleading results were observed (e.g., the PL intensity suppression due to the presence of magnetic field) when the ZnS:0.05Mn nano-particles sample was magnetized over the extended time due to artifact effects (e.g., temperature and laser power drift). We observed that the magneto-optical spectrum stability is identical for both blue (paramagnetic state) and orange (ferromagnetic state) bands. Chernenko *et al.* proposed the spin-selective energy transfer from excitonic to Mn^{2+} ion state induced by a magnetic ordering model to understand the magneto-PL spectrum suppression.[30] However, that process may not occur if such photo-excited excitonic states preferentially assume a spin state that would modify the selection rules and inhibit luminescence intensity suppression.[30] It is clear from the studies conducted here that such a scenario is highly conceivable and realistic. However, a more refined ferromagnetic-induced magneto-luminescence model is needed to corroborate this claim and to account for the dynamics of excitonic complexes below T_C in ZnS:0.05Mn nano-particles and similar material systems.

IV. CONCLUSION

We synthesized 4-nm ZnS:0.05Mn particles via a straightforward chemical route at room temperature. These nanoparticles exhibited bifunctionality below the ferromagnetic-paramagnetic transition temperature of 30 K. Under the influence of an applied magnetic field up to 10 kOe (1 T), no suppression of the Mn^{2+} ion PL intensity in ZnS:0.05Mn was observed below 30 K. In addition, the stability of the internal manganese PL under the influence of an applied magnetic field in the ferromagnetic state was reasonably associated to the fact that the photoexcited excitonic states responsible for the energy transfer have a preferential spin state, which modifies the selection rules inhibiting any PL suppression. Although the dynamics of excitonic complexes below T_C is still unclear, this study offers experimental support to test and better understand some current ferromagnetic models proposed for low-dimensional DMS. Moreover, the results presented here bring forth new avenues to widen the range of applications of ZnS:Mn nanostructures not only in optoelectronics but also in spintronics.

ACKNOWLEDGMENTS

This work was supported in part by the Institute for Functional Nanomaterials (NSF Grant No. 1002410) and PR NASA EPSCoR (NASA Cooperative Agreement No. NNX13AB22A). We gratefully acknowledge the HRTEM images and SQUID data provided by Dr. Maxime J.-F. Guinel and Dr. Carlos Rinaldi, respectively. W.M.J. acknowledges the support from the NSF CAREER Award No. DMR-1056493.

[1]L. Chen, W. Heimbrodt, P. J. Klar, M. Froba, C. Ronning, and H.-A. K. von Nidda, Phys. Status Solidi B **247**, 2522 (2010).
[2]Y. Wang, N. Herron, K. Moller, and T. Bein, Solid State Commun. **77**, 33 (1991).
[3]S.-J. Cheng, Phys. Rev. B **77**, 115310 (2008).
[4]P. Kacman, Semicond. Sci. Technol. **16**, R25 (2001).
[5]K. M. Hanif, R. W. Meulenberg, and G. F. Strouse, J. Am. Chem. Soc. **124**, 11495 (2002).
[6]B. Martinez, F. Sandiumenge, L. Balcells, J. Arbiol, F. Sibieude, and C. Monty, Phys. Rev. B **72**, 165202 (2005).
[7]K. Sato and H. K. Yoshida, Phys. Status Solidi B **229**, 673 (2002).
[8]R. N. Bhargava, D. Gallaguer, and T. Welker, J. Lumin. **60**, 275 (1994).
[9]L. Chen, F. J. Brieler, M. Fröba, P. J. Klar, and W. Heimbrodt, Phys. Rev. B **75**, 241303 (2007).
[10]R. Thakar, Y. Chen, and P. T. Snee, Nano Lett. **7**, 3429 (2007).
[11]I. Sarkar, M. K. Sanyal, S. Takeyama, S. Kar, H. Hirayama, H. Mino, F. Komori, and S. Biswas, Phys. Rev. B **79**, 054410 (2009).
[12]I. Sarkar, M. K. Sanyal, S. Kar, S. Biswas, S. Banerjee, S. Chaudhuri, S. Takeyama, H. Mino, and F. Komori, Phys. Rev. B **75**, 224409 (2007).
[13]J. Beltran-Huarac, M. J.-F. Guinel, B. Weiner, and G. Morell, Mater. Lett. **98**, 108 (2013).
[14]J. Beltran-Huarac, R. Martinez, and R. Palai, *in Magnetoelectric Properties of BST/LSMO Particulate Composites*, edited by P. Paruch, E. Tsymbal, M. Rzchowski, and T. Tybell (Materials Research Society, 2011), Vol. 1368, p. 5.
[15]J.-P. Ge, J. Wang, H.-X. Zhang, X. Wang, Q. Peng, and Y.-D. Li, Adv. Funct. Mater. **15**, 303 (2005).
[16]Z. Quan, D. Yang, C. Li, D. Kong, P. Yang, Z. Cheng, and Y. Lin, Langmuir **25**, 10259 (2009).
[17]W. Chen, Z. Wang, Z. Lin, Y. Xu, and L. Lin, J. Mater. Sci. Technol. **13**, 397 (1997).
[18]F. H. Su, B. S. Ma, Z. L. Fang, K. Ding, G. H. Li, and W. Chen, J. Phys.: Condens. Matter **14**, 12657 (2002).
[19]J. Yu, H. Liu, Y. Wang, F. E. Fernandez, and W. Jia, J. Lumin. **76**, 252 (1998).
[20]K. Kosai, B. T. Fitzpatrick, H. G. Grimmeiss, R. N. Bhargava, and G. F. Neumak, Appl. Phys. Lett. **35**, 194 (1979).
[21]A. A. Bol and A. Meijerink, Phys. Rev. B **58**, R15997 (1998).
[22]*Matlab* code has been developed based on a simple multi-exponential function. It was found that the *Matlab* fitting routine strongly depends on the parameter d_{dot} with $V_{dot}=(\pi/6)\ d_{dot}^3$. The standard deviation was monitored using a "free-run" fitting mode. To improve the fitting accuracy and get more realistic outcomes, d_{dot} was extracted from the experimental analysis.
[23]Th. Förster, Z. Naturforsch. **4a**, 321 (1949).
[24]M. Godlewski, V. Yu. Ivanov, P. J. Bergman, B. Monemar, Z. Golacki, and G. Karczewski, J. Alloys Compd. **341**, 8 (2002).
[25]W. Q. Peng, S. C. Qu, G. W. Cong, X. Q. Zhang, and Z. G. Wang, J. Cryst. Growth **282**, 179 (2005).
[26]N. Tusjii, H. Kitazawa, and G. Kido, J. Appl. Phys. **93**, 6957 (2003).
[27]V. Bindilatti, E. ter Haar, N. F. Oliveira, Y. Shapira, and M. T. Liu, Phys. Rev. Lett. **80**, 5425 (1998).
[28]R. C. Myers, M. Poggio, N. P. Stern, A. C. Gossard, and D. D. Awschalom, Phys. Rev. Lett. **95**, 017204 (2005).
[29]K. Yanata, K. Suzuki, and Y. Oka, J. Appl. Phys. **73**, 4595 (1993).
[30]A. V. Chernenko, P. S. Dorozhkin, V. D. Kulakovskii, A. S. Brichkin, S. V. Ivanov, and A. A. Toropov, Phys. Rev. B **72**, 045302 (2005).